



# Facile Design of Superparamagnetic Core-Shell EDC-Ascorbate-Fe<sub>3</sub>O<sub>4</sub> Nanocomposites for Targeted Delivery of Doxorubicin to Triple Negative Breast Tumor by Fenton Reaction

S. H. Mirjalili,  Mohammad Reza Nateghi,\*  F. Kalantari-Fotooh

Department of Chemistry, Yazd Branch, Islamic Azad University, Yazd, Iran

\* Corresponding author's e-mail address: mnateghi@iauyazd.ac.ir

RECEIVED: May 14, 2023 \* REVISED: October 27, 2023 \* ACCEPTED: November 7, 2023

**Abstract:** Triple negative breast cancer (TNBC) phenotype accounts for its significant resistance to chemotherapy and other therapeutic procedures. So, the establishment of better and effective therapeutic procedures has become a challenge during recent years. Doxorubicin is a potent chemotherapeutic candidate but its prominent side effects can be subsided via its combination with nanocarriers. So, the present study was aimed to design ascorbic acid modified biopolymeric EDC/NHS-modified magnetic nanoparticles (MNP@MNP@AA-EDC/NHS-DOX for doxorubicin drug delivery to the triple negative breast cancers cell lines of MDA-MB-231, MDA-MB-468 and HCC1937. Monodisperse Fe<sub>3</sub>O<sub>4</sub> MNPs were prepared by chemical co-precipitation method. According to the SEM and DLS results, MNP@AA-EDC/NHS-DOX, MNPs@AA, MNP@AA-MNP@AA-EDC/NHS and MNP@AA-EDC/NHS-DOX had average particle diameter of 53, 79 and 95 nm, respectively. While, XRD analysis showed that the MNP material had the strongest Fe crystal peak, while surface modified MNP@AA-EDC/NHS-DOX did not alter the characteristic properties of MNPs. VSM magnetization analysis revealed that MNP@AA-EDC/NHS-DOX exhibited sufficient paramagnetic potential in the presence of external magnetic field. The TG analysis showed that thermal decomposition capacity of present nanocomposites was: MNPs > MNP@AA-EDC/NHS > AA-MNPs > MNP@AA-EDC/NHS-DOX. AA-modified MNPs did not completely lose their thermal stability as compared to other modifications. Alamar blue analysis revealed that the bare MNPs did have non-significant cytotoxicity in MDA-MB-231, MDA-MB-468 and HCC1937 cell lines ( $p > 0.001$ ). While, MNP@AA-EDC/NHS-DOX at 0.1, 1.0 and 10  $\mu\text{g/mL}$  DOX concentrations showed significantly lowered cell survival percentages as compared to the free DOX regimens after 24 and 72h. While, HCC1937 cell line had the most accumulation of free (1.42 > 0.93 > 0.9  $\mu\text{g DOX/cell}$ ) and conjugated DOX (2.64 > 2.2 > 1.91  $\mu\text{g DOX/cell}$ ) after 6 h of incubation period as compared to MDA-MB-468 and MDA-MB-231, respectively (\*  $p < 0.05$ ). Present results provide a new insight into the design of paramagnetic targeted drug delivery nanocomposite system to overcome the obstacles and side effects of conventional chemotherapeutic agents.

**Keywords:** triple negative breast cancer, ascorbic acid modified MNPs, ferromagnetism, doxorubicin, Fenton reaction.

## INTRODUCTION

**B**REAST cancer has been declared to be the commonest cancer type in females. While, triple negative breast cancer (TNBC) accounts for the 10–15 % of all breast cancer subtypes with a relative survival rate of 40 % within 5-years and has higher metastatic potential to distant parts of body.<sup>[1]</sup> TNBC tends to occur in black ethnic premenopausal women of under 40 years of age and does not exhibit estrogen receptor (ER), progesterone receptor (PR) and human epidermal growth factor receptor-2 (HER2) and

hence tests negative (ER<sup>-</sup>, PR<sup>-</sup>, HER2<sup>-</sup>) for all three proteins.<sup>[2]</sup> TNBC is classified as a sub-type of basal-like breast cancer (BLBC) according to the gene-expression profile analysis because of approximately 56–90 % overlap of expression profiles in both cancer subtypes.<sup>[3,4]</sup>

The molecular phenotype of TNBC makes it resistant to chemotherapy, adjuvant chemo-radiotherapy, hormone therapy and molecular targeted therapy. Furthermore, modern therapeutic approaches, like Bevacizumab use, have also failed to significantly increase patient's life span. So, the development of new and effective therapeutic

approaches has become a necessary target of researchers in recent years.<sup>[5–7]</sup> Doxorubicin is one of the most potent anticancer drugs used in chemotherapeutic practice against several solid tumors and exhibits potential cytotoxic, anticancer and cytostatic properties.<sup>[8]</sup> The most concerning side effect of this drug is its mechanism of action that it works by attacking fast growing cells such as cancer, hair, skin and stomach lining cells, while bone marrow depression, reduced immunity and cardiovascular toxicity are the most important adverse effects. Therefore, extensive research has been carried out to resolve the drug toxicity issues and enhancing its targeted delivery to cancerous tissues and therapeutic potential.<sup>[9]</sup>

One strategy for improving the antitumor selectivity and toxicity profile of cytotoxic anticancer therapeutic agents is the use of magnetic carriers.<sup>[10]</sup> On account of the concept of combination chemotherapy, co-delivery of anticancer drugs with nanotechnology gradually becomes a desired strategy.<sup>[11]</sup> Superparamagnetic iron oxide nanoparticles ( $\text{Fe}_3\text{O}_4$ ) with a core ranging from 10 nm to 100 nm in diameter are powerful drug targeting vehicles in various biomedical applications.<sup>[12,13]</sup> The magnetic nanoparticles can be modified through organic or inorganic coating agents, used for the loading and delivery of a broad spectrum of anticancer drugs, and actively or passively target the diseased cells and tissues under the influence of external magnetic field. While, traveling through blood circulation, these nano-moieties do not tend to exhibit any residual magnetic interaction at room temperature under the absence of magnetic field and their uptake through phagocytosis is easily facilitated in the body, which significantly reduces their biological toxicity. Therefore, they remain in the circulation after injection and pass through the capillary systems of organs and tissues avoiding vessel embolism and thrombosis.<sup>[14]</sup> Some of these nanoparticles coated by synthetic and natural polymers or stabilized in micro- and nanogels, colloidal systems, liposomes, micelles, and microcapsules or transferred by cationic lipids, polylysine, and protamine sulfate have low entrapment efficiency of drug molecules, release drug molecules immediately not at the appropriate site, or make the particle size larger than the desirable range. Therefore, they do not show enough stability and have tendency to aggregate which leads to toxicity.<sup>[15,16]</sup> Such formulations are predominantly taken up by phagocytes of the reticuloendothelial system and cleared from blood circulation before they are able to reach the site of the tumor cells and finally reduce the magnetic nanoparticles efficiency.<sup>[17]</sup> Recently various anticancer drugs including paclitaxel, methotrexate, mitoxantrone, and doxorubicin have been conjugated with magnetic nanoparticles to enhance tumor targeting.<sup>[18]</sup>

Nanotechnology deals with the vast applications of materials in the scale of 1–100 nm. Nanoparticles have

recently been widely used as non-toxic, stealth drug delivery vehicles.<sup>[19]</sup> Research on natural polymer and metal nanoparticles composites received much attention in recent years.<sup>[20,21]</sup> Films incorporating metal nanoparticles may combine the properties of nanoparticles and the characteristics of films to produce new attributes that are beyond the individual components leading to active composites.<sup>[22]</sup> The electronic and optical properties of nanoparticles coupled with the mechanical stability of polymer films are relevant in many applications.<sup>[23]</sup> Natural polymers exhibit non-toxic and biodegradable properties when used in nanocomposite-based drug delivery systems.<sup>[24]</sup>

So, the present study aims at the facile design of superparamagnetic core-shell EDC-Ascorbate- $\text{Fe}_3\text{O}_4$  nanocomposites for targeted delivery of doxorubicin to triple negative breast tumor MDA-MB-231, MDA-MB-468 and HCC1937 cells by Fenton reaction.

## MATERIALS AND METHODS

### Materials

All the chemicals utilized in the experiment: ferric trichloride ( $\text{FeCl}_3$ ), ferrous chloride ( $\text{FeCl}_2$ ), ascorbic acid ( $\text{C}_6\text{H}_8\text{O}_6$ ), N-hydroxysulfosuccinimide (sulfo-NHS) and 1-ethyl-3-(3-dimethylaminopropyl) carbodiimide hydrochloride (EDC) were of analytical grade, obtained from Sigma Aldrich (St. Louis, MO, USA), and used without further purification. Double-distilled water (DDW) was used throughout the experiments. All other chemicals and agents were used as received without further purification.

### Synthesis of Bare $\text{Fe}_3\text{O}_4$ Nanoparticles

Monodispersed bare  $\text{Fe}_3\text{O}_4$  magnetic nanoparticles (MNPs) were prepared by chemical co-precipitation method with slight modifications.<sup>[25]</sup> Briefly, 10 mL of a mixture of 0.1 M  $\text{FeCl}_3$  and 0.05M  $\text{FeCl}_2$  with a molar ratio of 2:1 was mixed under constant stirring in a round bottom flask, immersed in a water-bath. The resultant mixture was kept at 35 °C under  $\text{N}_2$  protection for 30 min to maintain inert atmosphere. Precipitation was carried out with drop-wise addition of 7 mL of 2M NaOH under constant stirring conditions where pH reached to ~11. The resultant magnetic  $\text{Fe}_3\text{O}_4$  nanoparticles were separated using 2500 gauss neodymium alloy magnet and non-magnetic nanoparticles were removed through centrifugation at 10,000 rpm. The resultant precipitates were washed thrice with nanopure water (NPW) and ethanol until their pH was maintained at 7.0 before drying at 50 °C for 24 h under high vacuum to get the final black powder of  $\text{Fe}_3\text{O}_4$  nanoparticles. The resultant precipitates were suspended in DDW and kept at 4 °C for further use.

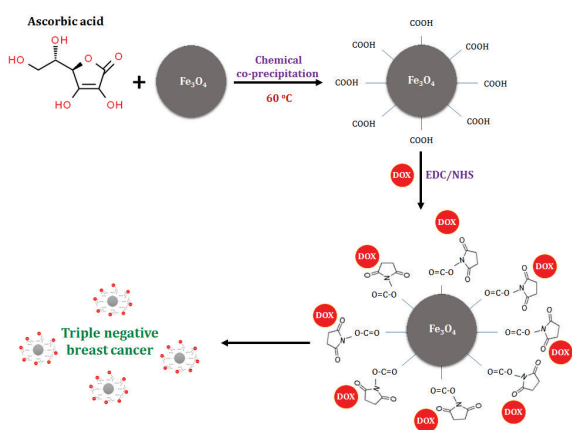
## Synthesis of Ascorbate-Functionalized Fe<sub>3</sub>O<sub>4</sub> Nanoparticles

Ascorbic acid-based carboxyl functionalization onto the MNPs surface was carried out according to the previous protocols with slight modifications.<sup>[26,27]</sup> Briefly, 70 mg of monodispersed MNPs were suspended in 20 mL DDW and sonicated for 30 min then, freshly prepared (560  $\mu$ L, 0.5 g mL<sup>-1</sup>) ascorbic acid solution was added while constantly stirring the mixture at 60 °C. The resultant reddish brown ascorbic acid-MNPs (AA-MNPs) precipitates were separated through 2500 gauss neodymium alloy magnet, cooled, washed thrice with nitrogen-purged DDW, centrifuged at 10.000 rpm for 5 minutes and dried for further use.

## EDC/NHS-Coupling and Drug Loading onto Ascorbate-Functionalized MNPs

As shown in Scheme 1, DOX was introduced to AA-MNPs via the EDC/NHS-mediated coupling reaction. The coupling was carried out following Dada et al. protocol with necessary modifications.<sup>[28]</sup> Briefly, 30 mg AA-MNPs were dispersed in 15 mL of 10 mM 2-(*N*-morpholino)ethanesulfonic acid (MES) buffer (pH = 5.5) and sonicated for 5 min. Then, the carboxyl groups of AA-MNPs were activated through EDC/sulfo-NHS (final concentration of 3.6 and 7.2 mM, respectively) while shaking for 2 h. Magnetic separation re-dispersion was carried out five times to wash excess EDC/NHS. The resulting solution was centrifuged at 8000 rpm for 10 min to remove unbound AA-MNPs, followed by re-dispersion in DDW and final magnetic separation. The resultant mixture was then freeze dried for further use.

Doxorubicin loading onto the EDC/NHS-based AA-MNPs (MNP@AA-EDC/NHS) was carried out through Yuan et al. (2017) protocol with slight modifications.<sup>[29]</sup> For this typical procedure, 1 mL of MNP@AA-EDC/NHS solution (8 mg mL<sup>-1</sup>), 1 mL of DOX solution (0.4 mg mL<sup>-1</sup>), and 2 mL of PBS (pH 7.4) were mixed and stirred together for 24 h at



**Scheme 1.** Schematic diagram of the synthesis and application of EDC/NHS coupled DOX-loaded AA-MNPs.

room temperature to a final concentration of 4 mL. Dialysis with dialysis membranes (molecular weight cutoff (MWCO) of 3.5 KDa) was done to remove the unreacted DOX or MNP@AA-EDC/NHS against 350 ml of deionized water for 2 h in dark. The final precipitated product was freeze dried for 48 h.

## Nanocomposite Characterization

### POWDER X-RAY DIFFRACTION (XRD)

XRD measurements were used to identify the crystalline phase of the particles before and after coating. XRD was performed on a Philips PW 1140/90 diffractometer using monochromatized x-ray beams from CuK $\alpha$ ,  $\lambda = 1.54 \text{ \AA}$  radiation at a scan rate of 1° min<sup>-1</sup> from 5° to 60° with a step size of 0.02°. The scanning voltage was 50KV, and the scanning current was 20 mA.

### VIBRATING SAMPLE MAGNETOMETRY (VSM)

The particular values for the inundation magnetization measurements were directly acquired on a predetermined weight of SPIONs before and after coating using Vibrating Sample Magnetometry (VSM, Princeton Applied Research, model ISS) working at room temperature. A recognized weight of the samples was placed into the VSM sample holder. A top magnetic field of approximately 15KOe was used. The saturation magnetization values were standardized to the mass of samples to yield specific magnetization, Ms (emu g<sup>-1</sup>).

### FOURIER TRANSFORM INFRARED SPECTROSCOPY (FTIR)

FTIR spectra of the nanoparticles were collected on an FTIR spectrophotometer using PerkinElmer Spectrum 100 Series FT-IR spectrometer in a wave number varying from 4000 to 400 cm<sup>-1</sup> with a resolution accuracy of 4 cm<sup>-1</sup> under ambient conditions. Before compacting, all samples were dried at 70 °C for 48 h. A small amount of each sample dry powder was thoroughly mixed and crushed with dried KBr using a mortar and pestle. The mixture was pressed into pellets using 8 tons cm<sup>-2</sup> of pressure for 2 minutes to form discs for analysis.

### SCANNING ELECTRON MICROSCOPY (SEM)

SEM was used to determine the size and morphology of the nanoparticles. The nanoparticle suspension was diluted, and a few drops were put on a carbon-stabilized grid (200 meshes). The grids were left in the oven at 50 °C overnight. Sample grids were attached to the sample holder on a Hitachi H7500 SEM instrument at an accelerating voltage of 15 kV microscope. The mean diameter of the size distribution was determined by measuring more than 150 particles from SEM images using Image J9.

### DYNAMIC LIGHT SCATTERING ANALYSIS OF HYDRODYNAMIC DIAMETER ASSESSMENT

Dynamic light scattering (DLS) measurements were carried out by Malvern Zetasizer Nano ZS through a 173° angle of backscatter analysis. A VWR® Symphony™ Ultrasonic Cleaner was employed to resuspend the MNP pellets and the resultant pellets were centrifuged at 8000 rpm to purify all the MNPs.

### DOX Loading Profile onto MNPs

EDC/NHS/AA-MNPs were first lyophilized at -86 °C and then freeze-dried using FreeZone benchtop freeze dryer machine (Labconco, Kansas, MO). Then, the Drug-loaded MNPs were dissolved in DMSO and the mass of DOX release from MNPs was compared with the standard curve of DOX in DMSO (3.5 mg mL<sup>-1</sup>). DOX loading and entrapment efficiency inside the MNP@AA-EDC/NHS-DOX were observed through fluorescence plate reader (BioTek H4 multimode plate reader) at λ<sub>Ex</sub> 500 nm, λ<sub>Em</sub> 600 nm. Drug loading was calculated by [Eq.(1)]:

$$\text{Drug loading (\%)} = \frac{\text{Mass of DOX in NPs}}{\text{Mass of NPs}} \times 100 \quad (1)$$

### pH Dependent Drug Release Profile

MNP@AA-EDC/NHS-DOX were diluted into PBS at pH 6.0 at a concentration equivalent to 5 μg mL<sup>-1</sup> free DOX (i.e. 8.6 μM DOX) and incubated at 37 and 42 °C (the normal physiological and the tumor microenvironment (TME) temperatures, respectively) for 0, 2, 4, 6, 8, 10 and 12 h. Free DOX dilution was also prepared in the same buffer for up to 5 μg mL<sup>-1</sup> concentration and incubated under the same conditions to serve as unbound control. After incubation and centrifugation at 20,000 × g to get NPs pellets, free DOX content in the supernatant was determined by fluorescence plate reader (BioTek H4 multimode plate reader) at λ<sub>Ex</sub> 500 nm, λ<sub>Em</sub> 600 nm. The percent DOX mass, released at each time point, was determined using a standard calibration curve of free DOX as a standard.

### Dose Response Cytotoxicity Analysis – Alamar Blue Assay

HCC1937 cells were maintained in ACL4 medium, supplemented with 10 % FBS, according to the Tomlinson et al. protocol.<sup>[30]</sup> MDA-MB-231, MDA-MB-468 cells were cultured at 1 × 10<sup>4</sup> cells/well were cultured in RPMI 1640 medium containing heat-inactivated FBS (10 %, v / v). Cells were then treated with free MNPs, free DOX (0.1, 1.0 and 10.0 μg mL<sup>-1</sup>) and MNP@AA-EDC/NHS-DOX at 0.1, 1.0 and 10 μg mL<sup>-1</sup> DOX for 6 h and then transferred to the drug-free fresh medium after washing thrice with PBS. Cell viability was determined at 24 and 72 h using the Alamar blue viability assay following the manufacturer's protocol (Invitrogen, Carlsbad, CA).

### Cellular Uptake of DOX Conjugates and Fluorescence Imaging

Cells were plated at 1 × 10<sup>5</sup> cells mL<sup>-1</sup> concentration in 10 % FBS supplemented RPMI-1640 culture medium per well in 96-well plates for 24 h. Cells were incubated with 10 μg mL<sup>-1</sup> free DOX or a concentration of NP-DOX equivalent to 10 μg mL<sup>-1</sup> free drug in 1 mL RPMI-1640 supplemented medium for 6 h before washing the cells thrice with PBS and transferring the cells to drug-free fresh medium. Alamar blue was used to determine cell number per well and calculated based on a previously prepared standard curve of Alamar blue reduction to plated cell number. At 6 h and 24 h time points after initiating drug treatment, cells were solubilized with 400 μL concentrated HCl and transferred to a black bottom 96-well plate for fluorescence measurement on the microplate reader. DOX concentration per cell was calculated based on DOX fluorescence and cell number obtained from Alamar blue reduction.

For the determination of cell fluorescence, 5 × 10<sup>5</sup> cells were plated in 1.5 mL supplemented RPMI-1640 medium per well in 6-well plates containing 22 × 22 mm glass cover slips. Cells were incubated with 10 μg mL<sup>-1</sup> free DOX or equimolar concentration of MNP@AA-EDC/NHS-DOX in 1.5 mL RPMI-1640 medium for 6 and 24 h. Cells were subsequently washed thrice with PBS before being transferred to drug-free medium. After incubation time, the cells were washed thrice with PBS and fixed in 4 % formaldehyde (Sigma Aldrich; St. Louis, Missouri, United States) for 30 min. Cell membranes were stained with wheat germ agglutinin, Alexa Fluor 488 conjugates (WGA-AF488, Invitrogen, Carlsbad, CA) according to the manufacturer's protocol. Cover slips were then mounted on microscope slides using Prolong Gold anti-fade solution (Invitrogen, Carlsbad, CA) containing DAPI for cell nuclei staining. Images were acquired on an inverted fluorescent microscope (Leica Microsystems Inc. Deerfield, IL 60015 United States) with the appropriate filters using a Nikon Ri1 Color Cooled Camera System (Nikon Instruments, Melville, NY) and 60× Oil Objective Lens (Nikon Instruments, Melville, NY).

### Statistical Analysis

One-way ANOVA statistical analysis with post hoc testing was used to evaluate the significance of the data. Probability levels less than 0.05 were taken to demonstrate significant differences, and the data were indicated by (\*) for *p* < 0.05 and (\*\*) for *p* < 0.001.

## RESULTS AND DISCUSSION

### Analysis of Morphology and Hydrodynamic Diameter

Scanning electron microscopy (SEM) and Dynamic Light Scattering (DLS) were used to characterize the microscopic

morphology of (A) AA-MNPs, (B) MNP@AA-EDC/NHS and (C) MNP@AA-EDC/NHS-DOX. The surface modification of MNPs with ascorbic acid provided the particles with non-aggregated surface area with average particle diameter of 53 nm (Figure 1A and B). The surface of AA-MNPs microscale aggregates is uneven and has irregular fixtures, which may be caused by the polymeric structure ascorbic acid residues and is favorable for the further surface modification with EDC/NHS and doxorubicin drug loading. While, the modified MNP@AA-EDC/NHS and MNP@AA-EDC/NHS-DOX (Figures 1C-F, respectively) exhibited more uniform spherical structures with average particle diameter of 79 and 95 nm, respectively.

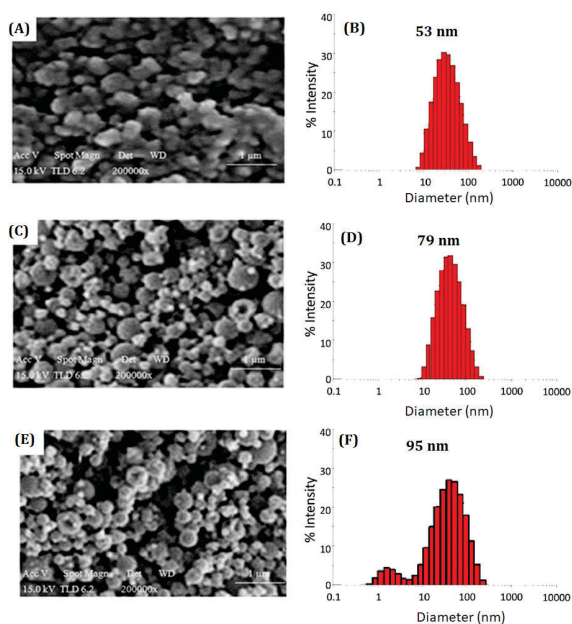


**Figure 1.** SEM images and DLS hydrodynamic diameter profiles of (A and B) MNP@AA, (C and D) MNP@AA-EDC/NHS and (E and F) MNP@AA-EDC/NHS-DOX, respectively.

**Table 1.** Polydispersity index (PDI) and Zeta ( $\zeta$ )-potential of MNPs.

	Z-average / nm / PDI <sup>(a)</sup>	$\zeta$ -potential / mV <sup>(b)</sup>	EE <sup>(c)</sup> / %	DL <sup>(d)</sup> / %
MNP@AA	53 / 0.23 $\pm$ 0.21	-11.4 $\pm$ 3.1	-	-
MNP@AA-EDC/NHS	79 / 0.22 $\pm$ 0.05	-10.5 $\pm$ 4.8	-	-
MNP@AA-EDC/NHS-DOX	95 / 0.23 $\pm$ 0.08	-7.8 $\pm$ 9.1	91 $\pm$ 2.74	38 $\pm$ 0.95

<sup>(a)</sup> Numbers are shown as averages  $\pm$  SD diameter of MNPs PDI values of multiple batches.

<sup>(b)</sup> Values are averages of multiple batches  $\pm$  average of  $\zeta$ -deviation taken from Malvern Zetasizer Nano ZS.

<sup>(c)</sup> EE = entrapment efficiency; DL = drug loading.

Table 1 shows the electrokinetic zeta ( $\zeta$ ) potential that can provide better understanding and prediction about the characteristics and interactions between nanoparticles in a suspension. The eta measurements were carried out at physiological pH (7.4). According to Table 1, the surface charge of the MNP@AA, MNP@AA-EDC/NHS and MNP@AA-EDC/NHS-DOX was found to be  $-11.4$ ,  $-10.5$  and  $-2.8$  mV, respectively. MNP@AA-EDC/NHS-DOX displayed high entrapment efficiency (EE) of  $91 \pm 2.74$  % with an effective DOX loading of  $38 \pm 0.95$  %.

## Powder XRD Characterization

As presented in Figure 2, the XRD analysis of different MNPs showed distinct peaks. The bare MNPs (Figure 2a) exhibited obvious characteristic peaks, because of the crystalline Fe species of magnetite ( $\text{Fe}_3\text{O}_4$ ). While, MNP@AA-EDC/NHS-DOX did not lose the characteristics of MNP peak intensity (Figure 2b), which shows that the surface modification of MNPs with biological antioxidant (ascorbic acid – AA), EDC/NHS polymers and doxorubicin did not alter the Fe crystalline structure and all polymers were successfully added to the MNPs after modification. Figure 1a showed the MNP material had the strongest Fe crystal peak, while surface modified MNP@AA-EDC/NHS-DOX did not alter the characteristic properties of MNPs.

## FT-IR Analysis

The characteristics of the functional groups and physical interactions between the components of bare and modified nanocomposites were obtained by the Fourier Transform infrared spectroscopy (FT-IR) spectra. In order to elucidate the interaction of ascorbic acid, loaded EDC/NHS polymers and DOX and with MNPs, separate FT-IR analyses were done. According to Figure 3, the Fe–O magnetic bond of bare magnetic nanoparticles produced sharp signals at

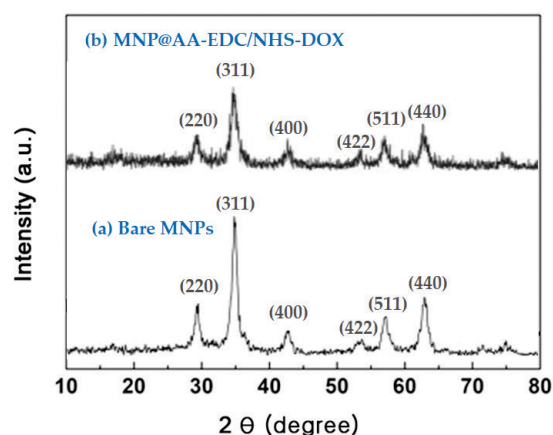


**Figure 2.** The XRD analysis of (a) bare MNPs and (b) MNP@AA-EDC/NHS-DOX.

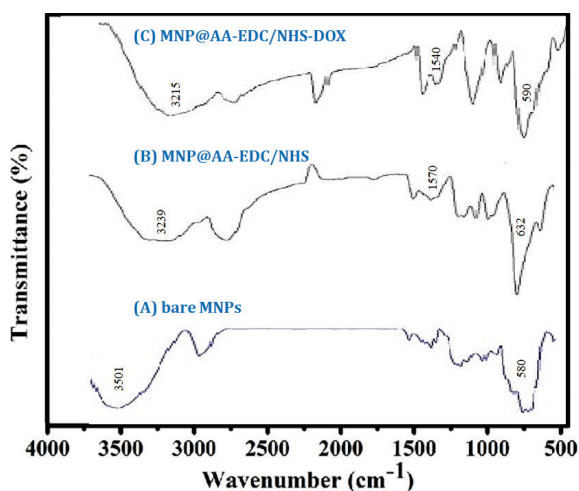


**Figure 3.** The FT-IR spectra of (a) bare MNPs, (b) MNP@AA-EDC/NHS and (c) MNP@AA-EDC/NHS-DOX.

580  $\text{cm}^{-1}$ , which it is attributed to supramagnetic properties of  $\text{Fe}_3\text{O}_4$  nanoparticles. While, O–H stretching was seen at 3501  $\text{cm}^{-1}$ . While, according to Figures 3B and C, shifted stretching vibrations of Fe–O were seen at 632 and 590  $\text{cm}^{-1}$ ; O–H stretching shifts were recorded at 3239 and 3215  $\text{cm}^{-1}$  and finally N-H bending vibrations in DOX and EDC/NHS moieties were recorded at 1540 and 1570  $\text{cm}^{-1}$ , respectively in MNP@AA-EDC/NHS and MNP@AA-EDC/NHS-DOX.

### Hysteresis Regression Analysis

The magnetization strength of AA, AA-MNPs, MNP@AA-EDC/NHS and MNP@AA-EDC/NHS-DOX was characterized after adsorption through the magnetic field. Figure 4 shows

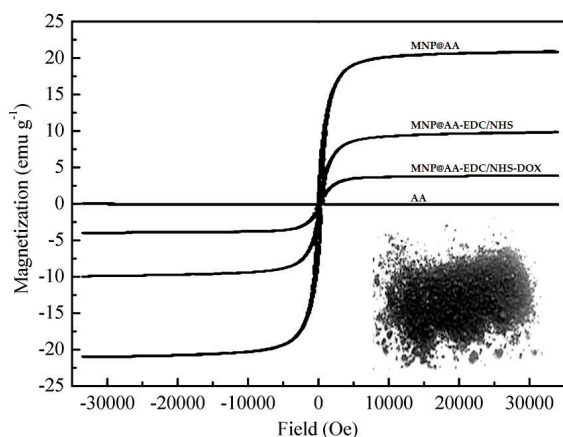


**Figure 4.** Magnetic hysteresis analysis. The hysteresis loops indicate the magnetization properties of AA-MNPs, MNP@AA-EDC/NHS, MNP@AA-EDC/NHS-DOX and AA at 298 K. Inset: The photograph of amorphous paramagnetic EDC/NHS@DOX/AA-MNP powder.

that the AA has almost no magnetization properties. However, the modification of MNPs with ascorbic acid (AA-MNPs) does not alter the magnetism of MNPs (20.4  $\text{emu g}^{-1}$ ). While, MNP@AA-EDC/NHS could reach its highest largest magnetization capacity level of 3.1  $\text{emu g}^{-1}$ , which was much lesser as compared to AA-MNPs. Moreover, MNP@AA-EDC/NHS-DOX had a much higher magnetization capacity of 10.2  $\text{emu g}^{-1}$ , which shows that DOX loading onto the MNP@AA-EDC/NHS enhanced the material's magnetism that can be attributed to the stabilization of negative charge of MNPs surface with positive charge of DOX and that could strengthen the NP's magnetization properties. Our results show that MNP@AA-EDC/NHS-DOX exhibit sufficient paramagnetic potential via the external magnetic field. While, the suspended MNP@AA-EDC/NHS-DOX could be readily collected by the external magnetic field (figure not shown).

### Thermogravimetric Analysis

The alterations in stability of MNPs before and after applying surface modification and drug loading is shown in Figure 5. According to the present results, thermal decomposition capacity of present nanocomposites was as follows: MNPs > MNP@AA-EDC/NHS > AA-MNPs > MNP@AA-EDC/NHS-DOX. The results show that the MNPs did not decompose until the temperature reached 400 °C, indicating their strong thermal stability. But the weight of MNP@AA-EDC/NHS > AA-MNPs > MNP@AA-EDC/NHS-DOX dropped sharply between 400 °C to 600 °C, indicating that they still had certain volatility and thermal instability, and the weight loss of AA-MNPs was most evident, which can be attributed to the vulnerable biopolymer of ascorbic acid. The lowest thermal stability of AA-MNPs can also be attributed to the oxidation of AA in the presence of MNPs, which caused a gradual decline of weight as the temperature increased to 800 °C. The TG analysis shows that AA-modified MNPs did

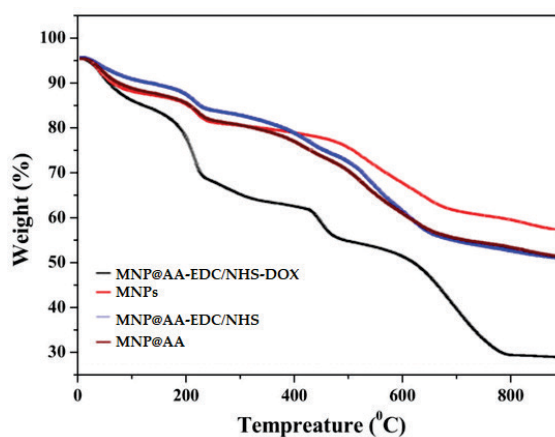


**Figure 5.** TG analysis of bare MNPs, AA-MNPs, MNP@AA-EDC/NHS and MNP@AA-EDC/NHS-DOX.

not completely lose their thermal stability as compared to other modifications.

### Drug Release Profile

Drug release profile of the MNP@AA-EDC/NHS-DOX was determined against pure doxorubicin solution at pH 6.0 (TME pH) and two temperatures of 37 °C (physiological temperature) and 42 °C (TME temperature) for 0–12 h. According to Figure 6, pure DOX showed 7.4 % and 12.5 % release during 12 h at 42 and 37 °C, respectively. While, this drug showed significantly improved release from modified MNP@AA-EDC/NHS-DOX, which was recorded to be 22.5 % and 26.7 % during 12 h period at pH 6.0, 37 and 42 °C, respectively; which are near to the TME internal conditions.

### In Vitro Antineoplastic Potential Assessment

Cell survival percentages of MDA-MB-231, MDA-MB-468 and HCC1937 cell lines in the presence of free MNPs, free DOX (0.1, 1.0 and 10.0  $\mu\text{g mL}^{-1}$ ) and MNP@AA-EDC/NHS-DOX at 0.1, 1.0 and 10  $\mu\text{g mL}^{-1}$  DOX are shown in Figure 7. Our results show that bare MNPs did have non-significant cytotoxicity in all the above-stated cells ( $p > 0.001$ ). While, as compared to the free DOX regimens, the MNP@AA-EDC/NHS-DOX at 0.1, 1.0 and 10  $\mu\text{g mL}^{-1}$  DOX concentrations showed significantly lowered cell survival percentage. Of all the DOX concentrations, loaded onto polymer modified MNPs, 10  $\mu\text{g mL}^{-1}$  DOX group showed lowest cell survival profile after 24 h ( $* = p < 0.05$ ; as compared to control group) and 72 h ( $** = p < 0.001$ ; as compared to control group) of incubation (Figures 7A and B).

### Qualitative and Quantitative Intracellular DOX Accumulation Profile

To determine the ability of free and conjugated DOX to circumvent the ABC-mediated drug efflux, the quantitative drug accumulation in three TNBC drug resistant and ABC-overexpressing cell lines of MDA-MB-231, MDA-MB-468 and HCC1937 was carried out. Cells were incubated with 10  $\mu\text{g mL}^{-1}$  free DOX or an equivalent dose of MNP@AA-EDC/NHS-DOX for 6 and 24 h and then transferred to drug-free medium. As shown in Figure 8, HCC1937 cell line had the most accumulation of free (1.42 > 0.93 > 0.9 pg DOX/cell) and conjugated DOX (2.64 > 2.2 > 1.91 pg DOX/cell) after 6 h of incubation period as compared to MDA-MB-468 and MDA-MB-231, respectively ( $* p < 0.05$ ). By 24 h post initial drug exposure, DOX concentration in HCC1937, MDA-MB-468 and MDA-MB-231 cells treated with free drug (0.35 > 0.2 > 0.11 pg DOX/cell) was much less than the drug conjugated to the MNP@AA-EDC/NHS-DOX (1.2 > 0.95 > 0.89 pg DOX/cell), which clearly reflects different drug metabolism and efflux properties in three different TNBC cell lines ( $p < 0.001$ ; Figures 8A and B). These

findings may indicate that ABC transporter gene over-expression may impede the DOX accumulation in MDA-MB-231 cells > MDA-MB-468 cells.

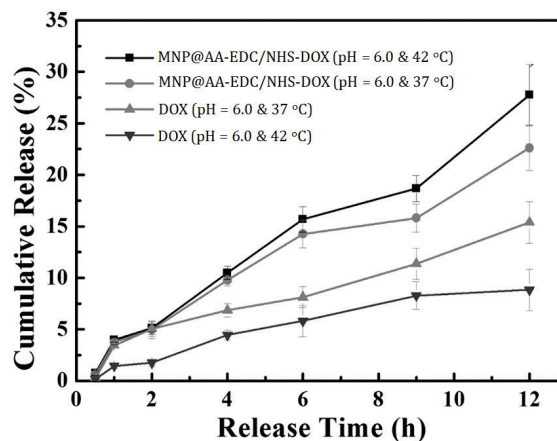


Figure 6. Drug release profile of MNP@AA-EDC/NHS-DOX at pH 6.0 and two temperatures; 37 and 42 °C for 0–12 h through dialysis.

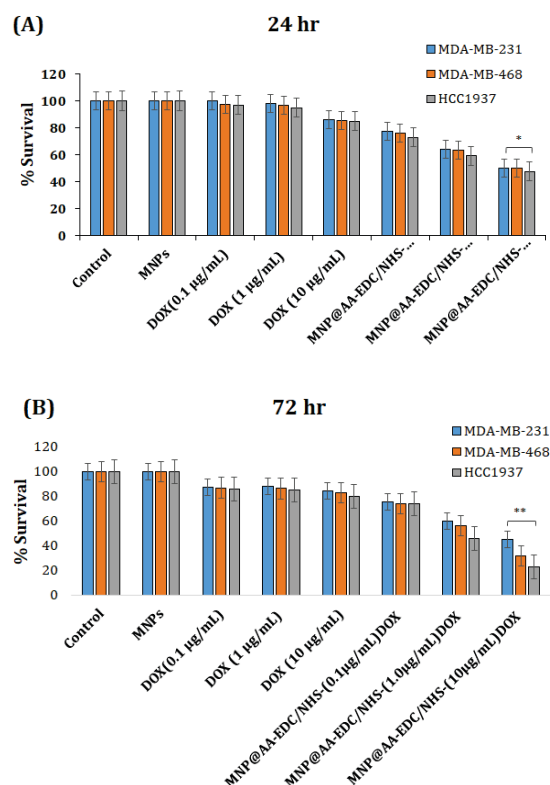
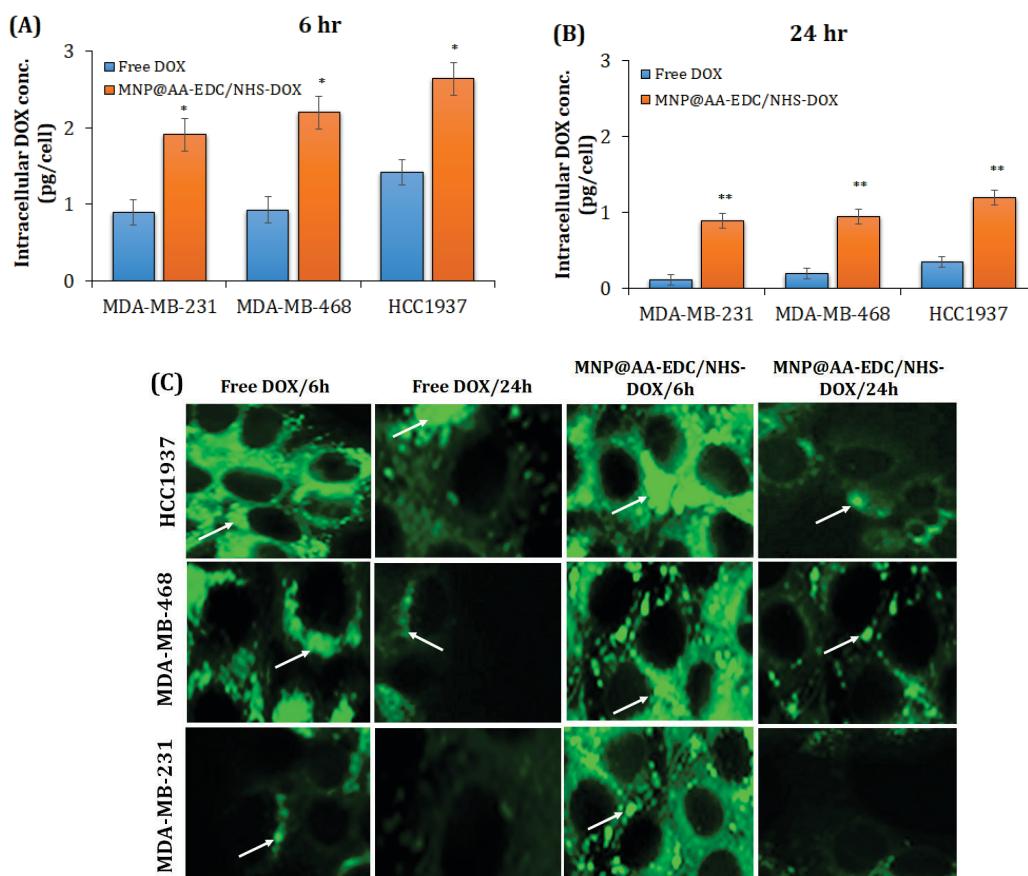


Figure 7. Alamar blue analysis of MNP, free DOX (0.1, 1.0 and 10  $\mu\text{g mL}^{-1}$ ) and MNP@AA-EDC/NHS-DOX (with 0.1, 1.0 and 10  $\mu\text{g mL}^{-1}$  concentrations of DOX) on TNBC cell lines of MDA-MB-231, MDA-MB-468 and HCC1937 type.

Consistent with the quantitative cellular uptake, MNP@AA-EDC/NHS-DOX showed a good internalization efficiency as compared to that of free DOX. The enhanced internalization of MNP@AA-EDC/NHS-DOX was evident from the bright green fluorescence of HCC1937 cell line after 6 h > 24 h of incubation as compared to MDA-MB-468 and MDA-MB-231 (Figure 8C, white arrow heads). This difference between the internalization potential as compared to free DOX is a direct consequence of the use of MNP@AA-EDC/NHS moieties for DOX loading, which may be attributed to the less negative ( $-2.8$  mV) zeta potential of MNP@AA-EDC/NHS-DOX nanocomposites as compared to MNP@AA and MNP@AA-EDC/NHS and their engulfment through cell's adsorptive endocytosis phenomenon.

MNP@AA-EDC/NHS-DOX were successfully prepared and mainly confirmed by increased hydrodynamic diameters through SEM and DLS (Figure 1) and obvious

changes of surface charges. The surface charge of the MNP@AA, MNP@AA-EDC/NHS and MNP@AA-EDC/NHS-DOX was recorded to be  $-11.4$ ,  $-10.5$  and  $-2.8$  mV, respectively. While the spherical nature (according to SEM analysis) is expected to permit their facile extravasation through the leaky tumor vasculature upon administration, resulting in passive accumulation of these nanocomposites into the tumor cells. Nanoparticles of the size range of  $\sim 10$ – $200$  nm are believed to provide prolonged blood circulation and passive targeting of their cargo drugs, thanks to the phenomenon of enhanced permeability and retention (EPR).<sup>[31]</sup> Currently, nanocarriers have great potential to specifically enhance drug accumulation in hypoxic tumor cells due to enhanced permeability and retention (EPR) effect.<sup>[32]</sup> Loading of drug molecules along with iron oxide nanoparticles within the coating material represents another approach of delivering a drug to the target site. This approach provides



**Figure 8.** Accumulation of free DOX or MNP@AA-EDC/NHS-DOX in three TNBC cell lines of MDA-MB-231, MDA-MB-468 and HCC1937. Cells were treated for with equimolar concentrations of  $1 \mu\text{g mL}^{-1}$  free or conjugated DOX for 6 and 24 h. The quantitative intracellular DOX was determined by the fluorescence of cell lysate and normalized to cell number using Alamar Blue at A) 6 h and B) 24 h after initial drug exposure. \* is  $p < 0.05$ , \*\* is  $p < 0.001$  as determined by Student's *t*-test. C) Qualitative cellular uptake analysis of free DOX and MNP@AA-EDC/NHS-DOX internalization through the three TNBC cell lines during 6 and 24 h incubation periods. White arrows represent the fluorescence of internalized drugs.



attractive solutions to problems such as low entrapment efficiency and stability. Particle size, surface coating, and surface charge are major determinants of the biodistribution, pharmacokinetics, and possible toxicity of SPIONs.<sup>[33]</sup>

Tissue distribution is mainly affected by particle size. SPIONs with a particle size smaller than 50 nm evade opsonization, thus increasing their circulation time and hence are gradually taken up by macrophages in the reticuloendothelial systems of the liver, lymph tissue, spleen, and bone marrow, whereas magnetic particles smaller than 50 nm are rapidly cleared from the bloodstream by sinusoidal Kupffer cells in the liver.<sup>[34]</sup> In addition to particle size, the coating material used on iron oxide particles also determines the rate of hepatic clearance. In general, SPIONs covered with coating materials which hinder access of water to the iron oxide core show slower degradation and hence an increased half-life in blood.<sup>[35]</sup> Surface charge, in addition to particle size and the coating material, affects the uptake of SPIONs by different cells. For instance, positively charged particles adhere nonspecifically to cells because the majority of the cell membranes have a net negative charge, whereas strong negative charges on the surface of magnetic particles facilitate their uptake by the liver.<sup>[35,36]</sup>

Schlorf et al. compared SPIONs with different core materials (magnetite, maghemite), different coatings (none, dextran, carboxy-dextran, and polystyrene) and different hydrodynamic diameters (20–850 nm) with regard to their internalization mechanisms, release of internalized particles, toxicity, and ability to generate contrast in MRI. For this study, they utilized U118 glioma cells and human umbilical vein endothelial cells exhibiting different phagocytic activity. Noncoated, carboxydextran-coated, and polystyrene-coated nanoparticles with a varying size range (10–850 nm) showed very nonspecific phagocytic uptake by tumor cells and endothelial cells. The coating and surface charge of the particles were demonstrated to exert a much larger influence on their nonspecific uptake than their size. Dextran-coated particles on the other hand were found to have completely different uptake behavior. The reason for this different uptake behavior was attributed to the dextran coating, making these nanoparticles suitable for specific labeling of molecular targets.<sup>[37]</sup> Our MNPs were coated with ascorbic acid to introduce the DHAA (dehydroascorbic acid) moieties onto the magnetic nanoparticles. These DHAA are actively internalized through endoplasmic reticulum of actively propagating cells (i.e; cancer cells) via their glucose transporter systems. So, ascorbate coating converts the nanoparticles into actively targeting particles.<sup>[38]</sup> While, modification of MNPs with EDC/NHS makes their surface more accessible to the drug molecules. Therapeutic potential of MNPs is caused by localized drug delivery to tumor tissues because of the deposition, accumulation, and retention of drug-conjugated

MNPs in tumors, enhanced by magnetic force. The amount of entrapped drug in the NP formulations was determined from the fluorescence intensity of Dox in dissolved NP solutions using fluorescence spectroscopy. Our results showed that DOX molecules were successfully loaded onto the MNP surface and had a considerable release kinetics.

Tumors cells exhibit a complex interaction with the surrounding stroma. TNBC cell line HCC1937 was first derived from a 24-years old female having a family history of breast cancer and a germ line mutation in BRCA1 and is characterized by homozygous deleterious mutations in BRCA1 gene.<sup>[39]</sup> Cancer cells grow in a disorganized mass of cells in culture systems. Moreover, different subtypes of breast cancer grow with distinct patterns. For instance, the basal B TNBC cell line MDA-MB-231 grows with a stellate pattern while the basal A TNBC cell line MDA-MB-468 TNBC grows with a grape cluster like pattern.<sup>[40]</sup> Accumulating evidence has reported that many TNBC tumors may display anoxic and/or hypoxic tissue areas that are heterogeneously distributed within the tumor mass. The oxygenation level in several cancers including breast cancer is found to be lower than that in the respective normal tissues.<sup>[41]</sup> It has been observed that when a tumor is growing, some regions of tumors undergo a decrease in O<sub>2</sub>, growth factors and glucose due to the poor vascularization of these regions.<sup>[42]</sup> In this study, we showed the evidence that MNP@AA-EDC/NHS-DOX induced cell death in TNBC cell lines via enhanced effect of loaded DOX (Figures 7 and 8).

Cell survival percentages of MDA-MB-231, MDA-MB-468 and HCC1937 cell lines were studied through Alamar Blue assay in the presence of free MNPs, free DOX (0.1, 1.0 and 10.0 µg mL<sup>-1</sup>) and MNP@AA-EDC/NHS-DOX at 0.1, 1.0 and 10 µg mL<sup>-1</sup> DOX. According to our results, bare MNPs did have non-significant cytotoxicity in all the above-stated cells. But, MNP@AA-EDC/NHS-DOX (at 10 µg mL<sup>-1</sup> DOX concentration) significantly reduced cell survival percentage (Figures 7A and B). MDA-MB-231 known to be a highly aggressive, invasive and poorly differentiated TNBC cell line because of the absence of expression of estrogen- (ER) and progesterone-receptor (PR) expression, as well as HER2 (human epidermal growth factor receptor 2) amplification.<sup>[4]</sup> Similar to other invasive cancer cell lines, the invasiveness of the MDA-MB-231 cells is mediated by proteolytic degradation of the extracellular matrix. Because of the lack of ER/PR, this cell line is known as 'basal' breast cancer cell line. Our Alamar Blue analysis also showed high resistance and more survival rate during 24 and 72 h of incubation periods.<sup>[43,44]</sup>

While, extent of ABC-mediated drug efflux mechanism in ABC-overexpressing cell lines of MDA-MB-231, MDA-MB-468 and HCC1937 showed that HCC1937 cell line had the most accumulation of free (1.42 > 0.93 > 0.9 µg DOX/cell) and conjugated DOX (2.64 > 2.2 > 1.91 µg

DOX/cell) after 6 h of incubation period as compared to MDA-MB-468 and MDA-MB-231, respectively. By 24 h post initial drug exposure, DOX concentration in HCC1937, MDA-MB-468 and MDA-MB-231 cells treated with free drug ( $0.35 > 0.2 > 0.11$  pg DOX/cell) was much less than the drug conjugated to the MNP@AA-EDC/NHS-DOX ( $1.2 > 0.95 > 0.89$  pg DOX/cell), which clearly reflects different drug metabolism and efflux properties in three different TNBC cell lines (Figures 8A and B). These findings indicate that ABC transporter gene over-expression may impede the DOX accumulation in MDA-MB-231 cells > MDA-MB-468 cells.

## CONCLUSION

Human cancer cell lines have been a useful tool for the study of the nano-biomedicine, genetics, molecular biology, biology, and therapy of cancer in many tumor types, including breast cancer. The TNBC cell lines mirror the original tumors from which they were derived morphologically and molecularly. Thus, they are useful for the study of molecular aberrations in TNBC and the study of the pathways affected by those aberrations. However therapeutic studies in TNBC have not readily translated into clinical results. TNBC and the cell lines derived from them represent a heterogeneous group of tumors. The challenge for the future is to understand the molecular pathways that drive transformation in different subsets of TNBC and then, using cell lines that are driven by the same pathways, to study how to manipulate them. Present results showed that MNP@AA-EDC/NHS-DOX induced cell death in TNBC cells. ascorbic acid decreased the resistance of TNBC cells to DOX because of its antioxidant potential, which indicates that the co-treatment of DOX with EDC/NHS@ AA-MNPs nanocomposites could be an effective approach to diminish cancer resistance to doxorubicin drug and resist tumor growth in TNBC.

## REFERENCES

- [1] N. U. Lin, *Cancer* **2018**, *113*, 2638–2645. <https://doi.org/10.1002/cncr.23930>
- [2] A. Goldhirsch, *Ann Oncol.* **2013**, *24*, 2206–2223.
- [3] A. Prat, E. Pineda, B. Adamo, P. Galván, A. Fernández, L. Gaba, M. Díez, M. Viladot, A. Arance, M. Muñoz, *Breast* **2015**, *24*, S26–35. <https://doi.org/10.1016/j.breast.2015.07.008>
- [4] L. Yin, J. J. Duan, X. W. Bian, *Breast Cancer Res.* **2020**, *22*, 61. <https://doi.org/10.1186/s13058-020-01296-5>
- [5] Y. Li, H. Zhang, Y. Merkhher, *J. Hematol. Oncol.* **2022**, *15*, 121. <https://doi.org/10.1186/s13045-022-01341-0>
- [6] S. Hwang, S. Park, Y. Kwon, *Pharmacol. Ther.* **2019**, *199*, 30–57. <https://doi.org/10.1016/j.pharmthera.2019.02.006>
- [7] L. Zhong, Y. Li, L. Xiong, *Sig. Transduct. Target. Ther.* **2021**, *6*, 201. <https://doi.org/10.1038/s41392-021-00572-w>
- [8] S. S. Qi, J. H. Sun, H. H. Yu, S. Q. Yu, *Drug Deliv.* **2017**, *24*, 1909–1926. <https://doi.org/10.1080/10717544.2017.1410256>
- [9] G. F. Weber, *Mol. Ther. Cancer.* **2014**, *8*, 9–12.
- [10] H. I. O. Gomes, C. S. M. Martins, J. A. V. Prior, *Nanomaterials (Basel).* **2021**, *11*, 964. <https://doi.org/10.3390/nano11040964>
- [11] P. Y. Teo, W. Cheng, J. L. Hedrick, Y. Y. Yang, *Adv. Drug Deliv. Rev.* **2016**, *98*, 41–63. <https://doi.org/10.1016/j.addr.2015.10.014>
- [12] Y. P. Yew, K. Shamelij, M. Miyake, N. Bahiyah, A. Khairudin, S. E. B. Mohamad, T. Naiki, K. X. Lee, *Arab. J. Chem.* **2020**, *13*, 2287–2308. <https://doi.org/10.1016/j.arabj.2018.04.013>
- [13] B. J. Tefft, S. Uthamaraj, J. J. Harburn, M. Klabusay, D. Dragomir-Daescu, G. S. Sandhu, *J. Vis. Exp.* **2015**, *19*, e53099.
- [14] E. Aram, M. Moeni, R. Abedizadeh, D. Sabour, H. Sadeghi-Abandansari, J. Gardy, A. Hassanpour, *Nanomater.* **2022**, *12*, 3567. <https://doi.org/10.3390/nano12203567>
- [15] J. Varshosaz, H. Sadeghi-aliabadi, S. Ghasemi, B. Behdadfar, *Biomed. Res. Int.* **2013**, 680712. <https://doi.org/10.1155/2013/680712>
- [16] Y. Zhang, T. Sun, C. Jiang, *Acta Pharm. Sin. B.* **2018**, *8*, 34–50. <https://doi.org/10.1016/j.apsb.2017.11.005>
- [17] Y. Tang, X. Wang, J. Li, Y. Nie, G. Liao, Y. Yu, C. Li, *ACS Nano.* **2019**, *13*, 13015–13026. <https://doi.org/10.1021/acsnano.9b05679>
- [18] M. Kenchegowda, M. Rahamathulla, U. Hani, M. Y. Begum, S. Guruswamy, R. A. M. Osmani, M. P. Gowrav, S. Alshehri, M. M. Ghoneim, A. Alshlowi, D. V. Gowda, *Molecules.* **2021**, *27*, 146. <https://doi.org/10.3390/molecules27010146>
- [19] S. Sim, N. K. Wong, *Biomed. Rep.* **2021**, *14*, 42. <https://doi.org/10.3892/br.2021.1418>
- [20] M. Elmowafy, K. Shalaby, M. H. Elkomy, O. A. Alsaïdan, H. A. M. Goma, M. A. Abdelgawad, E. M. Mostafa, *Polymers.* **2023**, *15*, 1123. <https://doi.org/10.3390/polym15051123>
- [21] M. El Rhazi, S. Majid, M. Elbasri, *Int. Nano Lett.* **2018**, *8*, 79–99. <https://doi.org/10.1007/s40089-018-0238-2>
- [22] R. Goyal, L. K. Macri, H. M. Kaplan, J. Kohn, *J. Cont. Rel.* **2016**, *240*, 77–92. <https://doi.org/10.1016/j.jconrel.2015.10.049>
- [23] V. N. Popok, *Thin Solid Films.* **2022**, *756*, 139359. <https://doi.org/10.1016/j.tsf.2022.139359>
- [24] S. L. Prabu, T. N. K. Suriyaprakash, *Nov. Appr. Drug Des. Dev.* **2017**, *3*, 1–5.

- [25] G. Gnanaprakash, S. Mahadevan, T. Jayakumar, P. Kalyanasundaram, John Philip, Baldev Raj, *Mater. Chem. Phys.* **2007**, *103*, 168–175.  
<https://doi.org/10.1016/j.matchemphys.2007.02.011>
- [26] V. Sreeja, K. N. Jayaprabha, P. A. Joy, *Appl. Nanosci.* **2015**, *5*, 435–441.
- [27] A. Sood, V. Arora, J. Shah, R. K. Kotnala, T. K. Jain. *J. Exp. Nanosci.* **2016**, *5*, 370–382.  
<https://doi.org/10.1080/17458080.2015.1066514>
- [28] S. N. Dada, G. K. Babanyinah, M. T. Tetteh, V. E. Palau, Z. F. Walls, K. Krishnan, Z. Croft, A. U. Khan, G. Liu, T. E. Wiese, E. Glotser, H. Mei, *ACS Omega.* **2022**, *27*, 23322–23331.  
<https://doi.org/10.1021/acsomega.2c01482>
- [29] Y. Yuan, B. Guo, L. Hao, N. Liu, Y. Lin, W. Guo, X. Li, B. Gu, *Colloids Surf. B.* **2017**, *159*, 349–359.  
<https://doi.org/10.1016/j.colsurfb.2017.07.030>
- [30] G. E. Tomlinson, T. T. Chen, V. A. Stastny, A. K. Virmani, M. A. Spillman, *Cancer Res.* **1998**, *58*, 3237–3242.
- [31] I. V. Zelepukin, O. Y. Griaznova, K. G. Shevchenko, A. V. Ivanov, E. V. Baidyuk, N. B. Serejnikova, A. B. Volovetskiy, S. M. Deyev, A. V. Zvyagin, *Nat Commun* **2022**, *13*, 6910.  
<https://doi.org/10.1038/s41467-022-34718-3>
- [32] J. Wu, *J. Pers. Med.* **2021**, *11*, 771.  
<https://doi.org/10.3390/jpm11080771>
- [33] C. Chouly, D. Pouliquen, I. Lucet, J. J. Jeune, P. Jallet, *J. Microencapsul.* **1996**, *13*, 245–255.  
<https://doi.org/10.3109/02652049609026013>
- [34] S. E. Barry, *Int J Hyperthermia.* **2008**, *24*, 451–466.  
<https://doi.org/10.1080/02656730802093679>
- [35] K. Briley-Saebo, A. Bjornerud, D. Grant, H. Ahlstrom, T. Berg, G. M. Kindberg, *Cell Tissue Res.* **2004**, *316*, 315–323.  
<https://doi.org/10.1007/s00441-004-0884-8>
- [36] R. Augustine, A. Hasan, R. Primavera, R. J. Wilson, A. S. Thakor, B. D. Kevadiya, *Materials Today Communications.* **2020**, *25*, 101692.  
<https://doi.org/10.1016/j.mtcomm.2020.101692>
- [37] T. Schlorf, M. Meincke, E. Kossel, C. C. Gluer, O. Jansen, R. Mentlein, *Int J Mol Sci.* **2020**, *12*, 12–23.  
<https://doi.org/10.3390/ijms12010012>
- [38] J. M. May, *Front. Biosci.* **1998**, *3*, d1–10.  
<https://doi.org/10.2741/A262>
- [39] K. M. Aw Yong, K. M. Ulintz, P. J. Caceres. *Sci. Rep.* **2020**, *10*, 5781.  
<https://doi.org/10.1038/s41598-020-62516-8>
- [40] K. J. Chavez, S. V. Garimella, S. Lipkowitz, *Breast Dis.* **2011**, *32*, 35–48.  
<https://doi.org/10.3233/BD-2010-0307>
- [41] F. Y. Cheng, C. H. Chan, B. J. Wang, Y. L. Yeh, Y. J. Wang, H. W. Chiu, *Cancers (Basel).* **2021**, *13*, 606.  
<https://doi.org/10.3390/cancers13040606>
- [42] D. W. Siemann, M. R. Horsman, *Pharmacol. Ther.* **2015**, *153*, 107–124.  
<https://doi.org/10.1016/j.pharmthera.2015.06.006>
- [43] S. Jafari, A. Jahanmir, Y. Bahramvand, S. Tahmasebi, M. Dallaki, E. Nasrollahi, *Iran. J. Med. Sci.* **2022**, *47*, 40–47.
- [44] B. C. Borges, P. A. Do Amaral, L. R. Soldi, V. L. Silva, F. C. De Souza, F. A. Cordeiro Da Luz, R. A. De Araújo, M. J. Silva, *Mol. Clin. Oncol.* **2022**, *16*, 93.  
<https://doi.org/10.3892/mco.2022.2526>